Tenth International Conference on Computational Fluid Dynamics (ICCFD10), Barcelona,Spain, July 9-13, 2018

ICCFD10-2018-0342

On a physically-consistent nonlinear subgrid-scale heat flux model for LES of buoyancy driven flows

F.X. Trias[1], F. Dabbagh[1,2], A. Gorobets[1,3] and A.Oliva[1]
Corresponding author: xavi@cttc.upc.edu

[1] Heat and Mass Transfer Technological Center (CTTC),
Technical University of Catalonia, C/Colom 11, 08222 Terrassa (Barcelona)
[2] Christian Doppler Laboratory for Multi-Scale Modeling of Multiphase Processes,
Johannes Kepler University, Altenbergerstraße 69, 4040 Linz, Austria
[3] Keldysh Institute of Applied Mathematics, 4A, Miusskaya Sq., Moscow 125047, Russia

Abstract: In this work, we plan to shed light on the following research question: *can we find a nonlinear tensorial subgrid-scale (SGS) heat flux model with good physical and numerical properties, such that we can obtain satisfactory predictions for buoyancy driven turbulent flows?* This is motivated by our recent findings showing that the classical (linear) eddy-diffusivity assumption, $\boldsymbol{q}^{eddy} \propto \nabla\overline{T}$, fails to provide a reasonable approximation for the SGS heat flux, $\boldsymbol{q} = \overline{\boldsymbol{u}T} - \overline{\boldsymbol{u}}\,\overline{T}$. This has been shown in our recent work [Dabbagh *et al.*, Phys. Fluids 29, 105103 (2017)] where SGS features have been studied *a priori* for a Rayleigh-Bénard convection (RBC). We have also concluded that nonlinear (or tensorial) models can give good approximations of the actual SGS heat flux. The nonlinear Leonard model, $\boldsymbol{q}^{nl} \propto \nabla\overline{\boldsymbol{u}}\nabla\overline{T}$, is an example thereof. However, this model is unstable and therefore it cannot be used as standalone SGS heat flux model. Apart from being numerically stable we also want to have the proper cubic near-wall behavior. Corrections in this regard will be presented together with *a priori/posteriori* studies of nonlinear SGS heat flux models for RBC. Results from LES simulations will be compared with the DNS results obtained in the on-going PRACE project *"Exploring new frontiers in Rayleigh-Bénard convection"*.

Keywords: LES, SGS models, buoyancy-driven flows, turbulence

1 Introduction

Turbulent flows driven by thermal buoyancy are present in many technological applications, such as governing flows in nuclear reactors, solar thermal power plants, indoor space heating and cooling, electronic devices, and convection in the atmosphere, oceans and deep mantle. Most of these flows are ruled by turbulent regime purely sustained by buoyancy, the reason that imparts a significant complexity into the flow system. Mainly, the chief dynamics therein such as the vortical structures and thermal plumes are essentially associated with immanent unsteadiness, energy nonequilibriums, strong pressure fluctuations and hardly interacted different size scales of motions [1]. Following the self-sustained cycle of the plumes, they produce alternative nonequilibriums between the buoyant production and the viscous dissipation, which are mainly compensated by the pressure transport mechanisms [2]. As a consequence, predicting the complex coherent dynamics in a turbulent buoyancy-driven flow derives formidable challenges, particularly within the scope of turbulence modeling.

Direct numerical simulations (DNS) have provided a fruitful knowledge about the problem in the fields of coherent dynamics and turbulence physics [3, 4]. Apart from overcoming the uncertainties pertaining to the experimental studies, DNS has allowed to investigate and resolve many queries in Rayleigh-Bénard convection (RBC) at relatively high Rayleigh (Ra) numbers [5, 6]. However, the full resolution of every generated

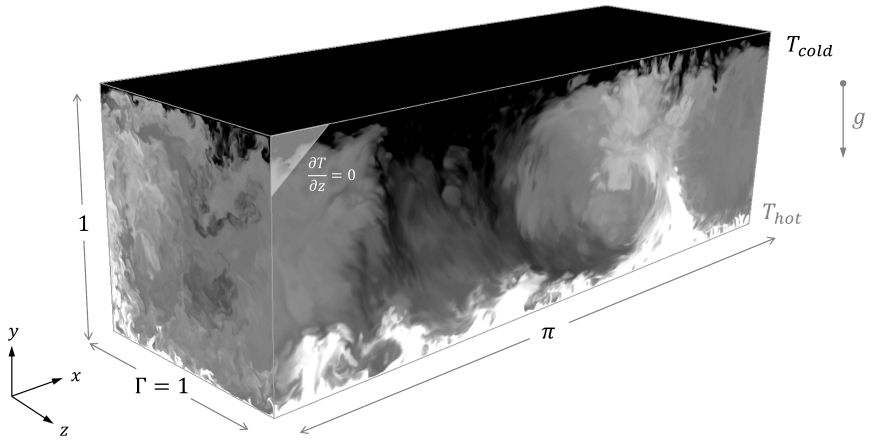

Figure 1: Schema of the Rayleigh-Bénard configuration studied in Refs. [4, 8]. Displayed together with a developed instantaneous temperature field taken of the DNS at $Ra = 10^{10}$.

vortical filament in DNS requires increasing computational demands with Ra. Therefore, in the foreseeable future, the numerical simulations of hard turbulent RBC will have to resort to turbulence modeling. We therefore turn to large-eddy simulation (LES) to predict the large-scale behavior of incompressible turbulent flows driven by buoyancy. In LES, the large scales of motions in a flow are explicitly computed, whereas effects of small-scale motions are modeled. Since the advent of computational fluid dynamics many subgrid-scale models have been proposed and successfully applied to a wide range of flows (see, for instance, the encyclopedic work of Sagaut [7]). The main goal of the current project is to improve the diffusive (linear) description of turbulent flows that is provided by eddy-diffusivity models for the subgrid-scale (SGS) heat flux. To that end, we will consider nonlinear SGS heat flux models that can properly represent the dynamics of the smallest (unresolved) scales, overcoming the inherent limitations of the eddy-diffusivity models [8]. Related with this, we also aim to find a proper definition of the subgrid characteristic length scale for simulations on anisotropic or unstructured grids. This is particularly important for highly anisotropic grids, on which the smallest grid spacing may start dominating the usually chosen characteristic length scale.

The specific SGS models that we consider consist of a linear eddy-viscosity term for momentum supplemented by a nonlinear model for the SGS heat flux. The model terms are designed to preserve important mathematical and physical properties, such as symmetries of the Navier-Stokes equations, and the near-wall scaling and the dissipative nature of the SGS. The desired properties are already included in existing models for the SGS stresses. Examples of eddy-viscosity models that exhibit the proper near-wall behavior are given by the WALE model [9], the σ-model [10] and the S3PQR model proposed in our previous work [11]. However, the (linear) eddy-diffusivity assumption fails to provide a reasonable approximation for the SGS heat flux. This has been clearly shown in our very recent work [8] where the SGS features have been studied *a priori* for a RBC at $Ra = 10^{10}$. We have also conclude that nonlinear (or tensorial) models can give a good approximation of the actual SGS heat flux. Among them, the models proposed by Daly and Harlow [12] (for RANS modeling) and Peng and Davidson [13] will be considered together with the new approach recently proposed on the basis of our *a priori* studies [8].

The rest of the paper is organized as follows. In the next section, the theoretical background of LES simulation of buoyancy-driven flows is presented. Then, in Section 3 different nonlinear SGS heat flux models are discussed and analyzed. Finally, conclusions are given in Section 4.

2 Background

2.1 Large-eddy simulation of buoyancy-driven flows

In large-eddy simulation, a filtering or coarse-graining operation is employed to distinguish between large and small scales of motion. This operation is denoted by an overbar in what follows. The evolution of the

incompressible large-scale velocity, $\overline{\boldsymbol{u}}$, and temperature, $\overline{T}$, fields can be described by the filtered Navier-Stokes and thermal energy equations, supplemented by the incompressibility constraint,

$$\partial_t \overline{\boldsymbol{u}} + (\overline{\boldsymbol{u}} \cdot \nabla)\overline{\boldsymbol{u}} = (Pr/Ra)^{1/2} \ \nabla^2 \overline{\boldsymbol{u}} - \nabla \overline{p} + \overline{\boldsymbol{f}} - \nabla \cdot \tau \ ; \qquad \nabla \cdot \overline{\boldsymbol{u}} = 0, \tag{1}$$

$$\partial_t \overline{T} + (\overline{\boldsymbol{u}} \cdot \nabla)\overline{T} = (Ra/Pr)^{-1/2} \nabla^2 \overline{T} \qquad\qquad - \nabla \cdot \boldsymbol{q}, \tag{2}$$

where $\overline{\boldsymbol{u}}$, $\overline{T}$ and $\overline{p}$ are respectively the filtered velocity, temperature and pressure. The SGS stress tensor, τ, and the SGS heat flux vector, $\boldsymbol{q}$, represents the effect of the unresolved scales,

$$\tau = \overline{\boldsymbol{u} \otimes \boldsymbol{u}} - \overline{\boldsymbol{u}} \otimes \overline{\boldsymbol{u}}, \tag{3}$$

$$\boldsymbol{q} \ = \overline{\boldsymbol{u} T} - \overline{\boldsymbol{u}}\,\overline{T}, \tag{4}$$

and they need to be modeled in order to close the system. The most popular approach is the eddy-viscosity assumption, where the SGS stress tensor is computed in alignment with the local rate-of-strain tensor, $\mathsf{S} = 1/2(\nabla \overline{\boldsymbol{u}} + \nabla \overline{\boldsymbol{u}}^t)$, *i.e.*

$$\tau \approx -2\nu_e \mathsf{S}(\overline{\boldsymbol{u}}). \tag{5}$$

In analogy to τ, the SGS heat flux is often approximated employing the gradient-diffusion hypothesis (linear modeling), given by

$$\boldsymbol{q} \approx -\kappa_t \nabla \overline{T} \qquad (\equiv \boldsymbol{q}^{eddy}). \tag{6}$$

Then, the Reynolds analogy assumption is applied to evaluate the eddy-diffusivity, κ_t: the heat flux is assumed to be analogous to the momentum flux and its ratio therefore, is constant. In this case, the eddy-diffusivity, κ_t, is derived from the eddy-viscosity, ν_e, by a constant turbulent Prandtl number, Pr_t, independent of the instantaneous flow conditions, *i.e.* $\kappa_t = \nu_e / Pr_t$. These assumptions have been shown to be erroneous to provide accurate predictions of the SGS heat flux in our recent work [8]. Namely, *a priori* analysis has shown that the eddy-diffusivity assumption, $\boldsymbol{q}^{eddy}$ (Eq. 6), is completely misaligned with the actual subgrid heat flux, $\boldsymbol{q}$ (see Figure 2, top left). In conclusion, one can corroborate the failure of the isotropic eddy-diffusivity parametrization ($\boldsymbol{q}^{eddy}$) in turbulent buoyancy driven flows. In contrast, the tensor diffusivity (nonlinear) Leonard model [14], which is obtained by taking the leading term of the Taylor series expansion of $\boldsymbol{q}$,

$$\boldsymbol{q} \approx \frac{\delta^2}{12} \mathsf{G} \nabla \overline{T} \qquad (\equiv \boldsymbol{q}^{nl}), \tag{7}$$

provides a much more accurate *a priori* representation of $\boldsymbol{q}$ (see Figure 2, top left). Here, G represents the gradient of the resolved velocity field, *i.e.* $\mathsf{G} \equiv \nabla \overline{\boldsymbol{u}}$. Then, the rate-of-strain, S, and the rate-of-rotation, Ω, tensors are respectively given by the symmetric and anti-symmetric parts,

$$\mathsf{S} = \frac{1}{2}(\mathsf{G} + \mathsf{G}^T) \qquad \Omega = \frac{1}{2}(\mathsf{G} - \mathsf{G}^T). \tag{8}$$

It can be argued that the rotational geometries are prevalent in the bulk region over the strain slots, *i.e.* $|\Omega| > |\mathsf{S}|$ (see Refs [4, 8]). Then, the dominant anti-symmetric tensor, Ω, rotates the thermal gradient vector, $\nabla \overline{T}$ to be almost perpendicular to $\boldsymbol{q}^{nl}$ (see Eq.7). Therefore, the eddy-diffusivity paradigm is only applicable in the not-so-frequent strain-dominated areas. This also matches with the observations of Chumakov [15], who performed *a priori* study of the SGS flux of a passive scalar in isotropic homogeneous turbulence.

2.2 Nonlinear SGS heat flux models for large-eddy simulation

Since the eddy-diffusivity, $\boldsymbol{q}^{eddy}$, cannot provide an accurate representation of the SGS heat flux, we turn our attention to nonlinear models. As mentioned above, the Leonard model [14] given in Eq.(7) can provide a very accurate *a priori* representation of the SGS heat flux (see Figure 2, top left). However, the local dissipation (in the L2-norm sense) is proportional to $\nabla T \cdot \mathsf{G} \nabla T = \nabla T \cdot \mathsf{S} \nabla T + \nabla T \cdot \Omega \nabla T = \nabla T \cdot \mathsf{S} \nabla T$. Since the velocity field is divergence-free, $\lambda_1^{\mathsf{S}} + \lambda_2^{\mathsf{S}} + \lambda_3^{\mathsf{S}} = 0$, and the eigensystem can be ordered $\lambda_1^{\mathsf{S}} \geqslant \lambda_2^{\mathsf{S}} \geqslant \lambda_3^{\mathsf{S}}$ with $\lambda_1^{\mathsf{S}} \geqslant 0$ (extensive eigendirection) and $\lambda_3^{\mathsf{S}} \leqslant 0$ (compressive eigendirection), and λ_2^{S} is either positive or negative. Hence, the local dissipation introduced by the model can take on negative values; therefore, the

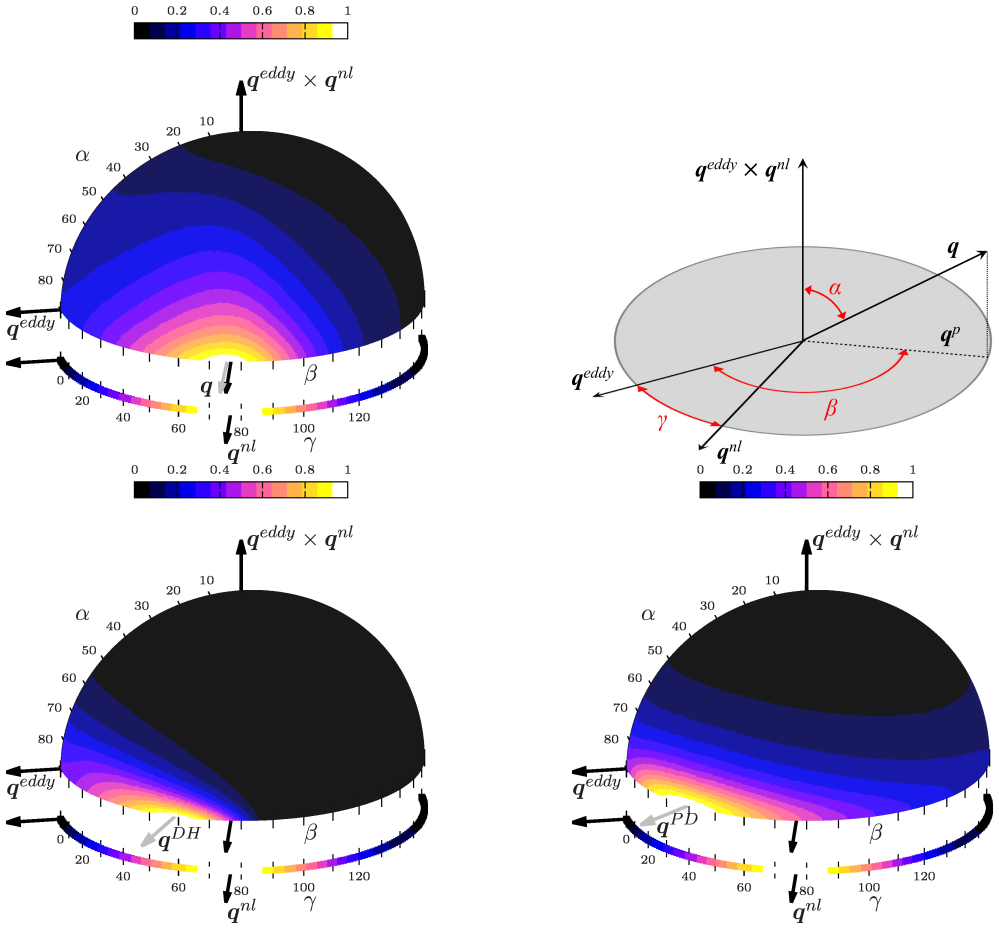

Figure 2: Joint probability distribution functions (PDF) of the angles (α, β) defined in the top right figure and plotted on a half unit sphere to show the orientation trends in the space of the mixed model. The PDF of γ is shown along the bottom strip of each chart. Alignment trends of the actual SGS heat flux, $\boldsymbol{q}$ (top, left), the Daly and Harlow [12] model (see $\boldsymbol{q}^{DH}$ in Eq. 11) (bottom, left) and the Peng and Davidson model [13] (see $\boldsymbol{q}^{PD}$ in Eq. 9) (bottom, right). For comparative and simplicity reasons, the JPDF and the PDF magnitudes are normalized by its maximal. For further details the reader is referred to our recent paper [8].

.

Leonard model cannot be used as a standalone SGS heat flux model, since it produces a finite-time blow-up. A similar problem is encountered with the nonlinear tensorial model proposed by Peng and Davidson [13],

$$\boldsymbol{q} \approx C_t \delta^2 \mathsf{S} \nabla T \qquad (\equiv \boldsymbol{q}^{PD}). \tag{9}$$

An attempt to overcome these instability issues is the so-called mixed model [16], where the Leonard model (Eq. 7) is linearly combined with an eddy-diffusivity model (Eq. 6),

$$\boldsymbol{q} \approx \frac{\delta^2}{12} \left(\mathsf{G} \nabla T - \Lambda |\mathsf{S}| \nabla T \right) \qquad (\equiv \boldsymbol{q}^{mix}), \tag{10}$$

where Λ is the ratio of the corresponding model coefficients. Another interesting nonlinear model was proposed by Daly and Harlow [12] for modeling the SGS heat flux for RANS,

$$\boldsymbol{q} \approx -\mathcal{T}_{SGS} \tau \nabla T = -\frac{1}{|\mathsf{S}|} \frac{\delta^2}{12} \mathsf{G} \mathsf{G}^T \nabla T \qquad (\equiv \boldsymbol{q}^{DH}), \tag{11}$$

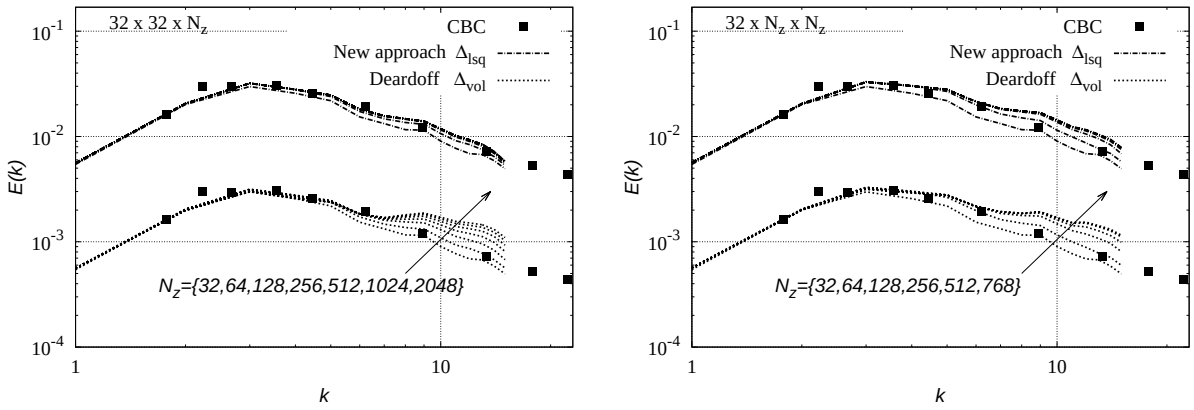

Figure 3: Energy spectra for decaying isotropic turbulence corresponding to the experiment of Comte-Bellot and Corrsin [18]. Results obtained with the new definition δ_{lsq} proposed in Eq.(27) are compared with the classical definition proposed by Deardorff given in Eq.(29). For clarity, latter results are shifted one decade down. For details the reader is referred to our recent paper [19].

where $\mathcal{T}_{SGS} = 1/|\mathsf{S}|$ is an appropriate SGS timescale [15] and the SGS stress tensor, τ, is approximated with the gradient model [17], *i.e.* $\tau \approx (\delta^2/12)\mathsf{G}\mathsf{G}^T$. Notice that the model proposed by Peng and Davidson (Eq. 9) can be viewed in the same framework if the SGS stress tensor is estimated by an eddy-viscosity model, *i.e.* $\tau \approx -2\nu_e\mathsf{S}$ and $\mathcal{T}_{SGS} \propto \delta^2/\nu_e$. These two models have shown a much better *a priori* alignment with the actual SGS heat flux (see Figure 2, bottom).

2.3 Wall-resolved LES: computational costs and mesh anisotropies. Choice of the characteristic length scale

In his 1979 pioneering paper, Chapman [20] estimated the number of grid points for an LES of turbulent boundary layers with and without wall modeling as

$$N_{wm} \sim Re_{L_x}^{2/5} \quad \text{and} \quad N_{wr} \sim Re_{L_x}^{9/5}, \tag{12}$$

respectively, where $Re_{L_x} = UL_x/\nu$ is the Reynolds number based on the free-stream velocity, U, and the flat plate length in the streamwise direction, L_x. To reach these scalings, Chapman used the following skin friction correlation

$$c_f = 0.045 Re_\delta^{-1/4}, \tag{13}$$

where $Re_\delta = U\delta/\nu$ is the Reynolds number based on the boundary layer thickness, $\delta(x)$, and assumed a seventh-power velocity distribution law, *i.e.* $u \sim y^{1/7}$. The later leads to an exact relation between the momemtum thickness, θ, and δ given by $\theta = 7\delta/72$. Then, using Eq.(13) and $c_f = 2d\theta/dx$ leads to

$$\frac{\delta}{x} = 0.37 Re_x^{-1/5} \quad \text{and} \quad c_f = 0.0577 Re_x^{-1/5}, \tag{14}$$

where $Re_x = Ux/\nu$ is the Reynolds number based on the streamwise distance from the leading edge, x. From these equations it is relatively easy to show the scaling given by Chapman in Eq.(12). Recently, Choi and Moin [21] gave new estimations based on a more accurate skin friction correlation for high Reynolds numbers ($10^6 \leq Re_x \leq 10^9$) given by

$$c_f = 0.020 Re_\delta^{-1/6}. \tag{15}$$

In this case, the analysis leads to

$$N_{wm} \sim Re_{L_x} \quad \text{and} \quad N_{wr} \sim Re_{L_x}^{13/7}. \tag{16}$$

These findings are extensively used to emphasize the prohibitive costs of LES without wall-modeling and the necessity, in the foreseeable future, of wall-modeling techniques for applications at high Reynolds numbers. However, under some assumptions, these scalings are only valid for a range of Re_x; moreover, they do not include the costs associated with temporal scales which eventually can be even more restrictive due to the inherent difficulty (impossibility?) to parallelize LES equations in time. These two issues are addressed in the next paragraphs. Let us consider a general power-law for the skin friction coefficient

$$c_f = aRe_\delta^\beta. \tag{17}$$

Then, following the above explained reasonings it leads to

$$\frac{\delta}{x} = bRe_x^\alpha \quad \text{and} \quad c_f = 7b/36(\alpha+1)Re_x^\alpha, \tag{18}$$

where $b = (36a(1-\beta)/7)^{1/(1-\beta)}$ and $\alpha = \beta/(1-\beta)$. Notice that with $a = 0.045$ and $\beta = -1/4$ it leads to the Chapman's scalings given in Eqs.(14). Following the same reasonings as in Ref.[21] the number of grid points in the outer layer and the viscous wall region can be estimated as follows

$$N^{out} = n_x n_y n_z \left(\frac{1}{b^2(1+2\alpha)}\right) \frac{L_z}{L_x} Re_{L_x}^{-2\alpha} \left(\left(\frac{Re_{L_x}}{Re_{x_0}}\right)^{1+2\alpha} - 1\right), \tag{19}$$

$$N^{vis} = \frac{n_y^w}{\Delta x_w^+ \Delta z_w^+} \frac{7b}{72} \frac{L_z}{L_x} Re_{L_x}^{2+\alpha} \left(1 - \left(\frac{Re_{x_0}}{Re_{L_x}}\right)^{1+\alpha}\right), \tag{20}$$

where $n_x n_y n_z$ is the number of grid points to resolve the cubic volume $\delta^3(x)$ in the outer layer (typically in the range $10^3 - 10^4$ [21]), L_z is the spanwise length and x_0 is the initial streamwise location where the skin friction correlation (18) holds. Then, Δx_w^+, Δz_w^+ and n_y^w are respectively the grid resolutions (in wall units) and the number of grid points in the wall-normal direction in the viscous wall region, *i.e.* $0 \le y^+ \lesssim l_y^+ \approx 100$. Typical values for WRLES lead to $n_y^w/(\Delta x_w^+ \Delta z_w^+) \sim 0.01$ [21]. This analysis can be extended giving estimations of the number of time-steps for the outer layer and the viscous wall region

$$N_t^{out} = \frac{N_{TU} n_x}{bC_{conv}} Re_{L_x} Re_{x_0}^{-(1+\alpha)}; \qquad N_t^{vis} = \max(N_{t_{diff}}^{vis}, N_{t_{conv}}^{vis}), \tag{21}$$

where

$$N_{t_{diff}}^{vis} = \frac{N_{TU}}{C_{diff}} \frac{7b}{72} \frac{\alpha+1}{(\Delta y_w^+)^2} Re_{L_x} Re_{x_0}^\alpha; \qquad N_{t_{conv}}^{vis} = \frac{N_{TU}}{C_{conv}} \sqrt{\frac{7b}{72} \frac{\alpha+1}{(\Delta x_w^+)^2}} Re_{L_x} Re_{x_0}^{\alpha/2}, \tag{22}$$

where N_{TU} is the number of time-units, L_x/U, to be computed; C_{conv} and C_{diff} are the convective and diffusive constants in the CFL condition. In summary, combining Eqs.(19), (20) and (21) leads to the following costs for LES with and without wall-modeling:

$$N_t^{wm} N_{wm} \sim Re_{L_x}^2 \quad \text{and} \quad N_t^{wr} N_{wr} \sim Re_{L_x}^{3+\alpha}. \tag{23}$$

Nowadays, this represents the main limitation of (wall-resolved) LES. On the other hand, it is also possible to give estimations of the mesh anisotropy, *i.e.* $\Delta x/\Delta y$, in the boundary layer. Namely, in the viscous sublayer, $\max(\Delta x/\Delta y) = \Delta x_w^+/\Delta y_w^+ \approx 50 - 100$ is not expected to change with the Reynolds number. However, in the overlap region ($y^+ \gtrsim 50$, $y/\delta < 0.1$) where control volumes of the viscous wall region and the outer layer ($y^+ \gtrsim 50$) must be smoothly connected, the grid anisotropy can be estimated as

$$\left(\frac{\Delta x}{\Delta y}\right)_{overlap} \approx \frac{(\Delta x)_{out}}{(\Delta y)_{vis}} = \frac{\delta}{n_x} \frac{n_y^w}{l_y}, \tag{24}$$

where l_y is the size of the viscous wall region, *i.e.* $l_y^+ = u_\tau l_y/\nu \approx 50 - 100$. Recalling the definition of the skin friction coefficient, $c_f = \tau_w/(\rho U^2/2)$, and using the relation given in Eq.(18), an expression in terms of

Re_x can be obtained

$$\left(\frac{\Delta x}{\Delta y}\right)_{overlap} \approx \frac{1}{\sqrt{2}}\frac{n_y^w}{n_x}\frac{b}{l_y^+}\sqrt{\frac{7b}{36}(\alpha+1)}Re_x^{1+3\alpha/2}. \tag{25}$$

Therefore, for any value of $\alpha > -2/3$ the mesh anisotropy, $\Delta x/\Delta y$, tends to grow with Re_x. Taking typical values for $n_x = 10$, $n_y^w = 20$ and $l_y^+ = 100$, and using, respectively, the skin friction coefficient correlations used by Chapman [20], *i.e.* $\alpha = -1/5$ and $b = 0.37$, and Choi and Moin [21], *i.e.* $\alpha = -1/7$ and $b = 0.17$, it simplifies

$$\left(\frac{\Delta x}{\Delta y}\right)_{overlap}^{Chapman} \approx 0.00125 Re_x^{7/10}\ ; \quad \left(\frac{\Delta x}{\Delta y}\right)_{overlap}^{Choi\&Moin} \approx 4.047\times 10^{-4} Re_x^{11/14}. \tag{26}$$

Just as examples, this leads to mesh anisotropies of 19.9 and 20.96 at $Re_x = 10^6$, and 99.7 and 127.97 at $Re_x = 10^7$. Therefore, numerical techniques that behave robustly in such meshes are of great interest.

In this context, the question that arises is how to compute the subgrid characteristic length, δ, that needs to be specified for all the models. It is usually associated with the local grid size. That is, for isotropic grids, δ is taken equal to the mesh size, $\delta = \Delta x = \Delta y = \Delta z$. However, for anisotropic or unstructured grids, a consensus has not been reached yet. With the aim to overcome the limitation of the Deardorff definition [22] (cube root of the cell volume), the following definition for δ was proposed and studied in a recent paper [19],

$$\delta_{\text{lsq}} = \sqrt{\frac{\mathsf{G}_\delta \mathsf{G}_\delta^T : \mathsf{G}\mathsf{G}^T}{\mathsf{G}\mathsf{G}^T : \mathsf{G}\mathsf{G}^T}}, \tag{27}$$

where $\mathsf{G} \equiv \nabla\overline{\boldsymbol{u}}$, $\mathsf{G}_\delta \equiv \mathsf{G}\Delta$ and $\Delta \equiv \text{diag}(\Delta x, \Delta y, \Delta z)$ (for a Cartesian grid). This definition of δ fulfills a set of desirable properties. Namely, it is locally defined and well bounded, $\Delta x \leq \delta_{\text{lsq}} \leq \Delta z$ (assuming that $\Delta x \leq \Delta y \leq \Delta z$). Moreover, it is sensitive to flow orientation and applicable to unstructured meshes (by simply replacing the tensor Δ by the Jacobian of the mapping from the physical to the computational space). This definition (27) is obtained minimizing (in a least-squares sense) the difference between the leading terms of the Taylor series of the SGS tensor, $\tau(\overline{\boldsymbol{u}})$, for an isotropic and an anisotropic filters lengths; namely,

$$\tau(\overline{\boldsymbol{u}}) = \frac{\delta^2}{12}\mathsf{G}\mathsf{G}^T + \mathcal{O}(\delta^4)\ ; \quad \tau(\overline{\boldsymbol{u}}) = \frac{1}{12}\mathsf{G}_\delta\mathsf{G}_\delta^T + \mathcal{O}(\delta^4), \tag{28}$$

Results displayed in Figure 3 correspond to the classical experimental results obtained by Comte-Bellot and Corrsin [18]. LES results have been obtained using the Smagorinsky model, for a set of (artificially) stretched meshes. In contrast with the results obtained using the Deardorff definition [22],

$$\delta_{\text{vol}} = (\Delta x \Delta y \Delta z)^{1/3}, \tag{29}$$

the proposed definition of the subgrid characteristic length, δ_{lsq}, significantly minimizes the effect of mesh anisotropies on the performance of SGS stress tensor models. For further details the reader is referred to our recent paper [19].

3 Building a proper SGS heat flux model

3.1 Exploring nonlinear SGS heat flux models

In this work we focus on finding a nonlinear SGS heat flux model with good physical and mathematical properties, that provides both accurate *a priori* representation of the actual SGS heat flux, $\boldsymbol{q}$, and satisfactory *a posteriori* predictions for turbulent buoyancy driven flows.

Let us remark that the focus of this study is not on the eddy-viscosity part of the model (see Eq. 5), but on the nonlinear approximation of the SGS heat flux, $\boldsymbol{q}$ (see Eq. 4). We do, however, have to make a specific choice for the SGS stress tensor model. We can, for instance, take one of the previously mentioned models: the WALE model [9], the σ-model [10] or the S3PQR models [11] (with the same near-wall scaling as the true turbulent stresses). Aiming to include several of the desirable properties according to which these

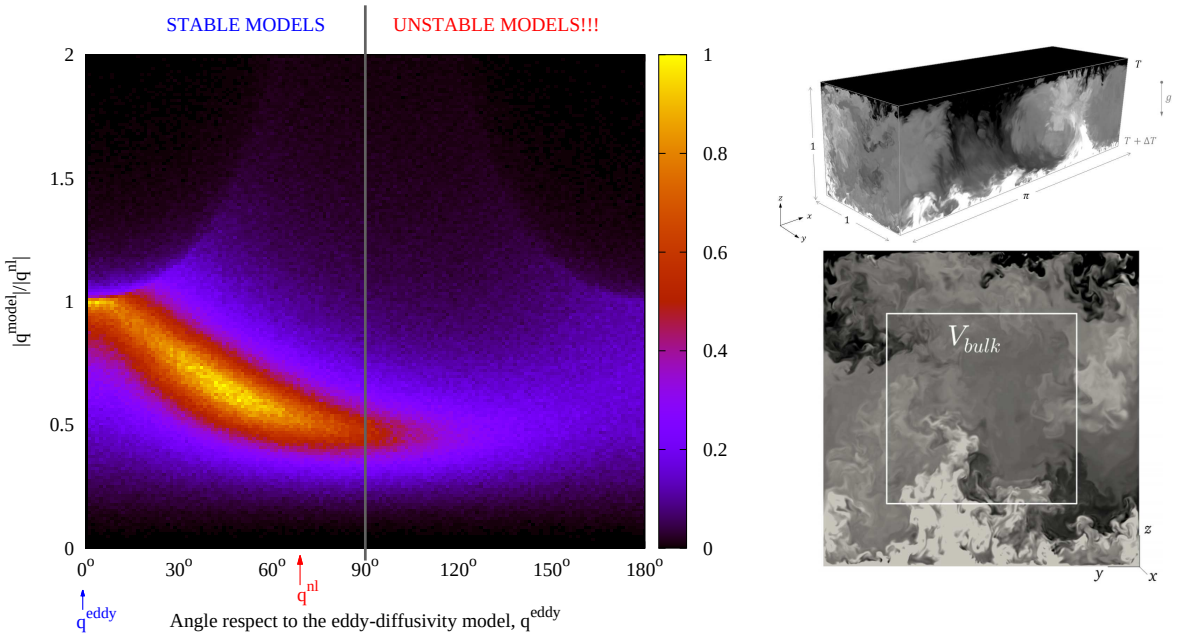

Figure 4: Joint PDF for the Peng and Davidson model (Eq. 9) in the space $(|\boldsymbol{q}^{PD}|/|\boldsymbol{q}^{nl}|, \beta)$ where the angle β is defined in Figure 2. The analized data corresponds to the bulk region of the air-filled Rayleigh-Bénard configuration at $Ra = 10^{10}$ studied in Refs. [4, 8].

models have been designed, we suggest to take the S3QR model proposed in our work [11],

$$\nu_e^{S3QR} = (C_{s3qr}\delta)^2 Q_{\mathsf{G}\mathsf{G}^T}^{-1} R_{\mathsf{G}\mathsf{G}^T}^{5/6}, \tag{30}$$

where $Q_{\mathsf{G}\mathsf{G}^T}$ and $R_{\mathsf{G}\mathsf{G}^T}$, are the second and the third invariants of the $\mathsf{G}\mathsf{G}^T$ tensor, respectively. This model exhibits the same near-wall scaling behavior as the turbulent stresses and it vanishes in all two-component flows, as well as in states of pure shear and pure rotation. Moreover, from a numerical point-of-view, it is solely based on the local flow topology contained in the tensor of the resolved velocity field, G, it is well-conditioned and it always provides non-negative values for $\nu_e \geq 0$.

As mentioned before, (linear) eddy-diffusivity (see Eq. 6) assumption cannot provide an accurate representation of the SGS heat flux, $\boldsymbol{q}$; hence, we turn our attention to nonlinear models. The least to be expected from a SGS model is to keep the stability of the numerical solution. This is not the case of the Leonard (Eq. 7) and the Peng and Davidson models (Eq. 9). Both of them have directions of negative diffusive that make the model numerical unstable. This is clearly observed in Figure 4 where the joint PDF for the Peng and Davidson model (Eq. 9) in the space $(|\boldsymbol{q}^{PD}|/|\boldsymbol{q}^{nl}|, \beta)$ is displayed. It is worth noticing that both models collapse to the same formula for $\beta = 0$, *i.e.* $\boldsymbol{q}^{PD} = \boldsymbol{q}^{nl} \propto \boldsymbol{q}^{eddy}$, since they corresponds to flows with null rate-of-rotation, $\Omega = 0$. This is also observed in Figure 4. On the other hand, the model proposed by Daly and Harlow [12] (see Eq. 11) does not suffer these problems since the tensor $\mathsf{G}\mathsf{G}^T$ is positive semi-definite. Moreover, this model has shown a rather good *a priori* alignment with the actual SGS heat flux (see Figure 2, bottom left). Therefore, hereafter we will consider nonlinear models based on the tensor, $\mathsf{G}\mathsf{G}^T$.

3.2 Near-wall scaling

It can be shown that due to the no-slip condition and the incompressibility constraint, the production of turbulent kinetic energy follows a cubic behavior near the wall [23], *i.e.* $y^+ \lesssim 5$. The major drawback of the classical Smagorinsky model is that the differential operator it is based on does not vanish in near-wall regions. First attempts to overcome this inherent problem of the Smagorinsky model made use of wall functions [24, 25]. However, the first outstanding improvement was the dynamic procedure proposed by

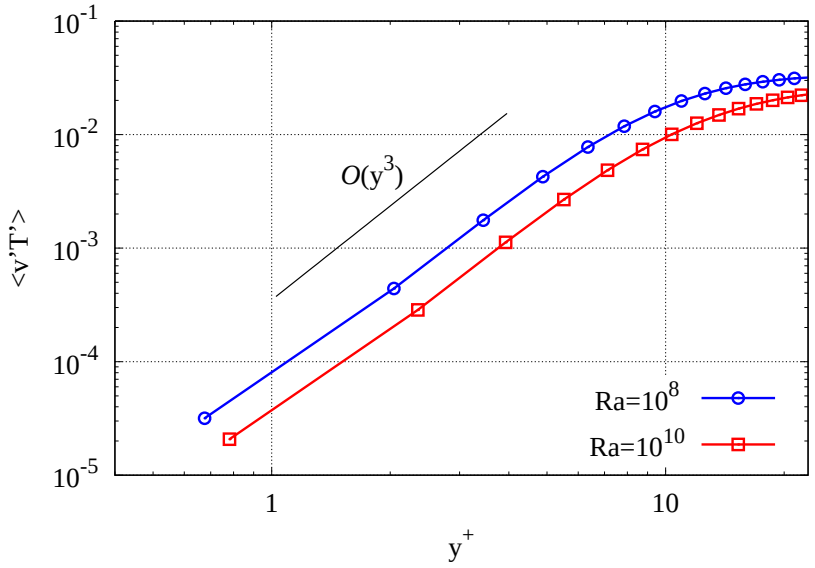

Figure 5: Near-wall scaling of $\langle v'T' \rangle$ for the air-filled Rayleigh-Bénard configurations at $Ra = 10^8$ and $Ra = 10^{10}$ studied on Refs. [4, 8].

Germano *et al.* [26] in the early 90s. Alternatively, it is possible to build models based on invariants that do not have this limitation. Examples thereof are the WALE [9], the Vreman's [27], the Verstappen's [28] and the σ-model [10] described in the previous section. This list can be completed with a novel eddy-viscosity model proposed by Ryu and Iaccarino [29] and two eddy-viscosity models recently proposed by the authors of this paper: namely, the S3PQR models [11] and the vortex-stretching-based eddy-viscosity model [30].

A similar analysis can be performed for the subgrid heat flux, $\boldsymbol{q}$. Namely, due to the no-slip condition and the incompressibility constraint, $\nabla \cdot \boldsymbol{u} = 0$, the stream-wise, wall-normal and span-wise velocity components and the temperature have the following scalings

$$u = ay + \mathcal{O}(y^2); \quad v = by^2 + \mathcal{O}(y^3); \quad w = cy + \mathcal{O}(y^2); \quad T = dy + \mathcal{O}(y^2), \tag{31}$$

where y is the distance to the wall and $a(x,z), b(x,z), c(x,z), d(x,z)$ are smooth functions that do not depend on y. Hence, the actual subgrid heat flux, $\boldsymbol{q}$, also follows a cubic behavior near the wall, *i.e.*

$$\boldsymbol{q} \propto \langle v'T' \rangle = \mathcal{O}(y^3). \tag{32}$$

The results displayed in Figure 5 confirms that this cubic scaling is valid for $y^+ \lesssim 8$. Let us consider now the near-wall scaling of the Daly and Harlow model given in Eq.(11),

$$G \propto \begin{pmatrix} y & 1 & y \\ y^2 & y & y^2 \\ y & 1 & y \end{pmatrix}; \ \nabla T \propto \begin{pmatrix} y \\ 1 \\ y \end{pmatrix} \implies \mathsf{G}\mathsf{G}^T \nabla \overline{T} \propto \begin{pmatrix} y \\ y^2 \\ y \end{pmatrix} = \mathcal{O}(y^1). \tag{33}$$

Therefore, the near-wall cubic behaviour is also recovered if the SGS timescale, $\mathcal{T}_{SGS}$, would scale quadratically. This is not the case of the timescale used in the Daly and Harlow [12] model, *i.e.* $\mathcal{T}_{SGS} = 1/|\mathsf{S}| = \mathcal{O}(y^0)$.

At this point it is interesting to observe that new timescales can be derived by imposing restrictions on the differential operators they are based on. For instance, let us consider models that are based on the invariants of the tensor $\mathsf{G}\mathsf{G}^T$

$$\boldsymbol{q} \approx -C_M \left(P^p_{\mathsf{G}\mathsf{G}^T} Q^q_{\mathsf{G}\mathsf{G}^T} R^r_{\mathsf{G}\mathsf{G}^T} \right) \frac{\delta^2}{12} \mathsf{G}\mathsf{G}^T \nabla T \qquad (\equiv \boldsymbol{q}^{S2}) \tag{34}$$

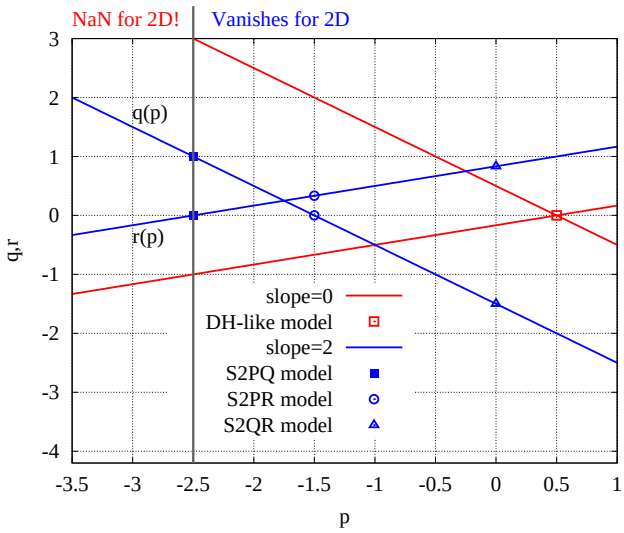

Figure 6: Near-wall scaling of $\langle v'T' \rangle$ for the air-filled Rayleigh-Bénard configurations at $Ra = 10^8$ and $Ra = 10^{10}$ studied on Refs. [4, 8].

	$P_{\mathsf{G}\mathsf{G}^T}$	$Q_{\mathsf{G}\mathsf{G}^T}$	$R_{\mathsf{G}\mathsf{G}^T}$
Formula	$2(Q_\Omega - Q_\mathsf{S})$	$V_\mathsf{G}^2 + Q_\mathsf{G}^2$	R_G^2
Wall-behavior	$\mathcal{O}(y^0)$	$\mathcal{O}(y^2)$	$\mathcal{O}(y^6)$
Units	$[T^{-2}]$	$[T^{-4}]$	$[T^{-6}]$

Table 1: Properties of the first, second and third invariants of the $\mathsf{G}\mathsf{G}^T$ tensor where $Q_\Omega = -1/2tr(\Omega^2)$, $Q_\mathsf{S} = -1/2tr\mathsf{S}^2$, $Q_\mathsf{G} = -1/2tr\mathsf{G}^2$ are the second invariants of Ω, S and G, respectively, and $R_\mathsf{G} = det(\mathsf{G})$ is the third invariants of G. Finally, the invariant V_G^2 is equal to the L^2-norm of the vortex-stretching term, *i.e.* $V_\mathsf{G}^2 = |\mathsf{S}\boldsymbol{\omega}|^2$. For further details the reader is referred to Ref. [11].

where $P_{\mathsf{G}\mathsf{G}^T}$, $Q_{\mathsf{G}\mathsf{G}^T}$ and $R_{\mathsf{G}\mathsf{G}^T}$ are the first, second and third invariant of the $\mathsf{G}\mathsf{G}^T$ tensor. This tensor is proportional to the gradient model [17] given by the leading term of the Taylor series expansion of the subgrid stress tensor $\tau(\overline{\boldsymbol{u}}) = (\delta^2/12)\mathsf{G}\mathsf{G}^T + \mathcal{O}(\delta^4)$. Formulae of these invariants, their wall behavior and their units are given in Table 1. Then, the exponents p, q and r in Eq.(34), must satisfy the following equations

$$-6r - 4q - 2p = 1; \qquad 6r + 2q = s, \tag{35}$$

to guarantee that the differential operator has units of time, *i.e.* $[P_{\mathsf{G}\mathsf{G}^T}^p Q_{\mathsf{G}\mathsf{G}^T}^q R_{\mathsf{G}\mathsf{G}^T}^r] = [T^1]$ and a slope s for the asymptotic near-wall behavior, *i.e.* $\mathcal{O}(y^s)$. Solutions for $q(p,s) = -(1+s)/2 - p$ and $r(p,s) = (2s+1)/6 + p/3$ are displayed in Figure 6. It we restrict ourselves to solutions with the proper near-wall scaling, *i.e.* $s = 2$ (blue lines in Figure 6), a family of p-dependent models follow. Hereafter, this family of models will be referred as S2PQR-model. Restricting ourselves to solutions involving only two invariants of $\mathsf{G}\mathsf{G}^T$ three models are found. Namely,

$$\boldsymbol{q}^{S2PQ} = -C_{s2pq} P_{\mathsf{G}\mathsf{G}^T}^{-5/2} Q_{\mathsf{G}\mathsf{G}^T} \frac{\delta^2}{12} \mathsf{G}\mathsf{G}^T \nabla\overline{T}, \tag{36}$$

$$\boldsymbol{q}^{S2PR} = -C_{s2pr} P_{\mathsf{G}\mathsf{G}^T}^{-3/2} R_{\mathsf{G}\mathsf{G}^T}^{1/3} \frac{\delta^2}{12} \mathsf{G}\mathsf{G}^T \nabla\overline{T}, \tag{37}$$

$$\boldsymbol{q}^{S2QR} = -C_{s2qr} Q_{\mathsf{G}\mathsf{G}^T}^{3/2} R_{\mathsf{G}\mathsf{G}^T}^{5/6} \frac{\delta^2}{12} \mathsf{G}\mathsf{G}^T \nabla\overline{T}, \tag{38}$$

for $p = -5/2$, $p = -1.5$ and $p = 0$, respectively. These three solutions are also represented in Figure 6. The

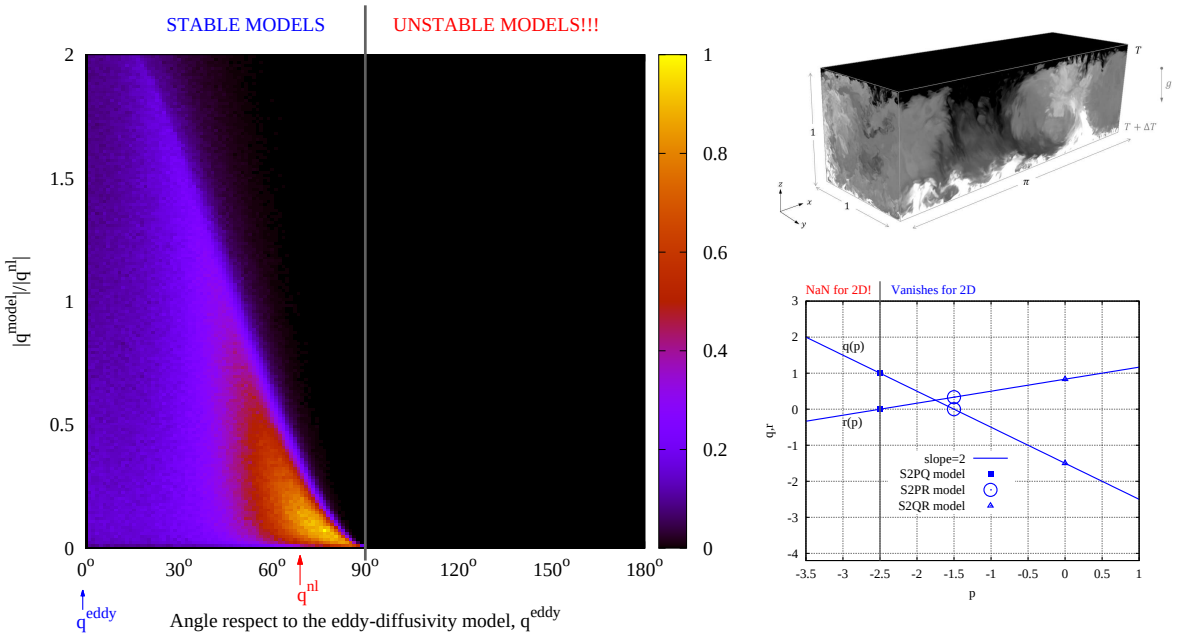

Figure 7: Joint PDF for the S2PR model (Eq. 37) in the space $(|\boldsymbol{q}^{PD}|/|\boldsymbol{q}^{nl}|, \beta)$ where the angle β is defined in Figure 2. The analized data corresponds to the bulk region of the air-filled Rayleigh-Bénard configuration at $Ra = 10^{10}$ studied in Refs. [4, 8].

alingment trends of all these three new models have also been studied *a priori*. For the sake of brevity, only results for the S2PR (Eq. 37) are shown in Figure 7. Apart from being unconditionally stable, this model displays the best alignment with the actual subgrid heat flux, $\boldsymbol{q}$. Hence, we consider that this a very good candidate for *a posteriori* LES simulations of buoyancy-driven flows.

4 Concluding remarks and future research

Motivated by our recent findings showing that the classical (linear) eddy-diffusivity assumption, $\boldsymbol{q}^{eddy} \propto \nabla\overline{T}$, fails to provide a reasonable approximation for the SGS heat flux, $\boldsymbol{q} = \overline{\boldsymbol{u}T} - \overline{\boldsymbol{u}}\,\overline{T}$ (see Figure 2), in this work we plan to shed light on the following research question: *can we find a nonlinear SGS heat flux model with good physical and numerical properties, such that we can obtain satisfactory predictions for a turbulent Rayleigh-Bénard convection?* We aim to answer this question by first studying the capability of the eddy-viscosity assumption (see Eq. 5) to model the SGS stress tensor, τ, without any modelization of the SGS heat flux. To do so, we will carry out LES simulations for very low Pr numbers. In this case, the ratio between the Kolmogorov length scale and the Obukhov-Corrsin length scale is given by $Pr^{1/2}$ [7]; therefore, for a $Pr = 0.005$ (liquid sodium) we have a separation of more than one decade. Hence, it is possible to combine a LES simulation for the velocity field, $\overline{\boldsymbol{u}}$, with the numerical resolution of all the relevant scales of the thermal field, T. Furthermore, we will study the performance of the above-mentioned nonlinear SGS heat flux models. Results from LES simulations will be compared with those obtained from DNS. In this regard, it is expected to play an important role the results obtained from the on-going PRACE supercomputing project *"Exploring new frontiers in Rayleigh-Bénard convection"* awarded with 33.1Mh in last PRACE 15th call. Results will be presented during the conference.

Acknowledgments

This work has been financially supported by the *Ministerio de Economía y Competitividad*, Spain (ENE2017-88697-R). F.X.T. is supported by a *Ramón y Cajal* postdoctoral contract (RYC-2012-11996) financed by

the *Ministerio de Economía y Competitividad*, Spain. F.D. is supported by the Tishreen University, Syria. A.G. is supported by the Russian Science Foundation (project 15-11-30039). This work has been carried out using computing resources of the Barcelona Supercomputing Center. The authors thankfully acknowledge these institutions.

References

[1] K. Hanjalić. One-point closure models for buoyancy-driven turbulent flows. *Annual Reviews of Fluid Mechanics*, 34:321–347, 2002.

[2] R. Togni, A. Cimarelli, and E. D Angelis. Physical and scale-by-scale analysis of Rayleigh-Bénard convection. *Journal of Fluid Mechanics*, 782:380–404, 2015.

[3] F. Chillà and J. Schumacher. New perspectives in turbulent Rayleigh-Bénard convection. *The European Physics Journal E*, 35:58, 2012.

[4] F. Dabbagh, F. X. Trias, A. Gorobets, and A. Oliva. On the evolution of flow topology in turbulent Rayleigh-Bénard convection. *Physics of Fluids*, 28:115105, 2016.

[5] R.J.A.M. Stevens, D. Lohse, and R. Verzicco. Prandtl and Rayleigh number dependence of heat transport in high Rayleigh number thermal convection. *Journal of Fluid Mechanics*, 688:31–43, 2011.

[6] E. P. van der Poel, R. Verzicco, S. Grossmann, and D. Lohse. Plume emission statistics in turbulent Rayleigh- Bénard convection. *Journal of Fluid Mechanics*, 772:5–15, 2015.

[7] P. Sagaut. *Large Eddy Simulation for Incompressible Flows: An Introduction*. Springer, third edition, 2005.

[8] F. Dabbagh, F. X. Trias, A. Gorobets, and A. Oliva. A priori study of subgrid-scale features in turbulent Rayleigh-Bénard convection. *Physics of Fluids*, 29:105103, 2017.

[9] F. Nicoud and F. Ducros. Subgrid-scale stress modelling based on the square of the velocity gradient tensor. *Flow, Turbulence and Combustion*, 62(3):183–200, 1999.

[10] F. Nicoud, H. B. Toda, O. Cabrit, S. Bose, and J. Lee. Using singular values to build a subgrid-scale model for large eddy simulations. *Physics of Fluids*, 23(8):085106, 2011.

[11] F. X. Trias, D. Folch, A. Gorobets, and A. Oliva. Building proper invariants for eddy-viscosity subgrid-scale models. *Physics of Fluids*, 27(6):065103, 2015.

[12] B. J. Daly and F. H. Harlow. Transport equations in turbulence. *Physics of Fluids*, 13:2634, 1970.

[13] S. Peng and L. Davidson. On a subgrid-scale heat flux model for large eddy simulation of turbulent thermal flow. *International Journal of Heat and Mass Transfer*, 45:1393–1405, 2002.

[14] A. Leonard. Large-eddy simulation of chaotic convection and beyond. *AIAA paper*, 97-0304, 1997.

[15] S. G. Chumakov. "*A priori* study of subgrid-scale flux of a passive scalar in isotropic homogeneous turbulence. *Physical Review E*, 78:036313, 2008.

[16] C. W. Higgins, M. B. Parlange, and C. Meneveau. The heat flux and the temperature gradient in the lower atmosphere. *Geophysical Research Letter*, 31:L22105, 2004.

[17] R. A. Clark, J. H. Ferziger, and W. C. Reynolds. Evaluation of subgrid-scale models using an accurately simulated turbulent flow. *Journal Fluid Mechanics*, 91:1–16, 1979.

[18] G. Comte-Bellot and S. Corrsin. Simple Eulerian time correlation of full- and narrow-band velocity signals in grid-generated, isotropic turbulence. *Journal of Fluid Mechanics*, 48:273–337, 1971.

[19] F. X. Trias, A. Gorobets, M. H. Silvis, R. W. C. P. Verstappen, and A. Oliva. A new subgrid characteristic length for turbulence simulations on anisotropic grids. *Physics of Fluids*, 26:115109, 2017.

[20] D. R. Chapman. Computational aerodynamics development and outlook. *AIAA Journal*, 17(12):1293–1313, 1979.

[21] H. Choi P. Moin. Grid-point requirements for large eddy simulation: Chapman's estimates revisited. *Physics of Fluids*, 24(1), 2012.

[22] J. W. Deardorff. Numerical study of three-dimensional turbulent channel flow at large Reynolds numbers. *Journal of Fluid Mechanics*, 41:453–480, 1970.

[23] D. R. Chapman and G. D. Kuhn. The limiting behaviour of turbulence near a wall. *Journal of Fluid Mechanics*, 170:265–292, 1986.

[24] P. Moin and J. Kim. Numerical investigations of turbulent channel flow. *Journal of Fluid Mechanics*, 118:341–377, 1982.

[25] U. Piomelli, J. Ferziger, P. Moin, and J. Kim. New approximate boundary conditions for large eddy simulations of wall-bounded flows. *Physics of Fluids A*, 1:1061–1068, 1989.

[26] M. Germano, U. Piomelli, P. Moin, and W. H. Cabot. A dynamic subgrid-scale eddy viscosity model. *Physics of Fluids*, 3:1760–1765, July 1991.

[27] A. W. Vreman. An eddy-viscosity subgrid-scale model for turbulent shear flow: Algebraic theory and applications. *Physics of Fluids*, 16(10):3670–3681, 2004.

[28] R. Verstappen. When does eddy viscosity damp subfilter scales sufficiently? *Journal of Scientific Computing*, 49(1):94–110, 2011.

[29] S. Ryu and G. Iaccarino. A subgrid-scale eddy-viscosity model based on the volumetric strain-stretching. *Physics of Fluids*, 26(6):065107, 2014.

[30] M. H. Silvis, R. A. Remmerswaal, and R. Verstappen. Physical consistency of subgrid-scale models for large-eddy simulation of incompressible turbulent flows. *Physics of Fluids*, 29(1):015105, 2017.